Published in final edited form as:

Dev Dyn. 2020 June ; 249(6): 775–788. doi:10.1002/dvdy.159.

Mammalian hemicentin 1 is assembled into tracks in the extracellular matrix of multiple tissues

Meei-Hua Lin[1], **Bill D. Pope III**[1], **Takako Sasaki**[2], **Daniel P. Keeley**[3], **David R. Sherwood**[3], **Jeffrey H. Miner**[1,4]

[1]Division of Nephrology, Department of Medicine, Washington University School of Medicine, St. Louis, Missouri, USA

[2]Department of Biochemistry II, Oita University, Oita, Japan

[3]Department of Biology, Regeneration Next, Duke University, Durham, North Carolina, USA

[4]Department of Cell Biology and Physiology, Washington University School of Medicine, St. Louis, Missouri, USA

Abstract

Background: Hemicentins (HMCNs) are a family of extracellular matrix proteins first identified in *C. elegans*, with two orthologs (HMCN1 and 2) in vertebrates. In worms, HMCN is deposited at specific sites where it forms long, fine tracks that link two tissues by connecting adjacent basement membranes (BMs). By generating CRISPR/Cas9-mediated *Hmcn1* and *Hmcn2* knockout mice, we tested the hypothesis that HMCNs perform similar functions in mammals.

Results: *Hmcn1−/−* mice were viable and fertile. Using new, knockout mouse-validated HMCN1 antibodies, HMCN1 was detected in wild-type mice as fine tracks along the BM of hair and whisker follicles, in the sclera of the eyes, and in the lumen of some lymphoid conduits. It was also observed in the mesangial matrix of the kidney glomerulus. However, HMCN1 deficiency did not affect the functions of these tissues, including adherence of coat hairs and whiskers, the sieving function of lymphoid conduits, or the immune response to injected antigens. HMCN2 deficiency did not lead to any discernible phenotypes on its own or when combined with HMCN1 deficiency.

Conclusion: That *Hmcn1−/−*, *Hmcn2−/−*, and *Hmcn1/2* double knockout mice did not display any overt phenotypes implicates compensation by other members of the fibulin family.

Keywords

basement membrane; matrix protein; whisker follicle; hair follicle; lymphoid conduits; sclera

1 | INTRODUCTION

Hemicentin (HMCN) is a member of the fibulin family of extracellular matrix proteins that was first identified in *C. elegans* [1,2] HMCNs are large ~5,000 amino acid proteins that

Correspondence: Jeffrey H. Miner, Division of Nephrology, Campus Box 8126, 4523 Clayton Ave., St. Louis, MO 63110, USA. Tel: 314-362-8235; Fax: 314-362-8237; minerj@wustl.edu.

consist of a single Von Willebrand A (VWA) domain at the amino terminus, followed by a HMCN motif, then approximately 50 immunoglobulin domains, and finally a series of epidermal growth factor (EGF) repeats and a single fibulin-like carboxyl-terminal module.[3] There is a single *Hmcn* gene in *C. elegans*, also referred to as *him-4*, and two vertebrate orthologues, *Hmcn1* (also called Fibulin-6) and *Hmcn2*.[4]

Localization studies and mutant analysis in *C. elegans* have indicated that HMCN mediates diverse cell-cell, cell-matrix and whole tissue adhesive and structural interactions. HMCN assembles into a variety of track-like structures that form directly on cells to stabilize cellular adhesions, such as neuronal-epidermal attachments, as well as extracellular scaffolds that support germ cell differentiation. HMCN also forms tracks along basement membranes (BM) that regulate the positioning and attachment of tissues to the epidermis, including the intestine, gonad, muscle, and uterus.[2,5,6]

In several locations in *C. elegans* HMCN is a component of a BM-BM adhesion complex, called a B-LINK, which spans adjoining BMs that connects tissues.[7] HMCN molecules can self-associate through interactions between EGF and fibulin-like domains.[8] The VWA domain of HMCN, which binds other matrix proteins,[9] may allow HMCN polymers to directly connect juxtaposed tissues through their BMs. The B-LINK adhesion complex also contains several other proteins, including the transmembrane integrin heterodimer INA-1/PAT-3 and the integrin binding cytolinker plakin (VAB-10A).[7] HMCN-mediated BM connections can be transient, such as a brief connection between the uterine and vulval BMs to align a cell invasion event that fuses the vulval with the uterine epithelium. Alternatively, they can be highly stable, such as the connection between the uterine-epidermal BM that holds the uterine tissue in the body cavity during egg-laying. Many aspects of the B-LINK adhesion system remain unknown, and genetic screens have suggested that numerous other proteins likely participate in B-LINK formation.[10] A role for HMCN in mediating BM-BM connections may be common across species, as mutant zebrafish carrying premature stop codon mutations in *Hmcn1* and zebrafish with *Hmcn1* knocked down both have defects in linking adjoining BMs in the epidermal folds that form developing fins.[11] Furthermore, knockdown of *Hmcn*2 in combination with genetic loss of fibulin 1 in zebrafish disrupts the BM-BM connection between the somite and epidermis.[12] In *C. elegans*, *him-4* worms carrying nonsense mutations in *Hmcn* manifest a failure in cytokinesis of germ cells and embryos, defective cell migration, and tissue fragility.[2] Notably, in *C. elegans*, the HMCN and fibulin-1 proteins directly interact, and fibulin-1 requires HMCN to localize at the B-LINK that connects uterine tissue to the epidermis.[5] Together these observations support the idea that HMCN (and possibly fibulin-1) might be shared components of an adhesion system that links adjoining tissues through BM-BM adhesions.

BM-BM adhesion between distinct tissues or structures within tissues commonly occurs during vertebrate development and in adult tissues. In this regard, of particular interest is the kidney glomerular BM (GBM), which arises from linkage and eventual fusion of an epithelial BM made by podocytes to one made by glomerular endothelial cells to establish the glomerular filtration barrier.[10,13] The mechanisms that facilitate BM connections in vertebrates are largely unknown, and it is unclear if HMCNs might similarly form tracks along BMs that help connect tissues. In zebrafish *Hmcn1* transcripts are expressed in

epidermal cells of developing fins, though HMCN1's localization is undetermined.[11] In contrast, zebrafish *Hmcn2* transcripts are mainly detected in mesenchymal cells of developing fins, with HMCN2 secreted to the local and the more apical regions.[12] In mice HMCN1 and 2 were reported to be deposited in the pericellular matrix of several tissues, based on results from an antibody raised against the VWA domain of *C. elegans* HMCN and recognizing both mouse HMCN1 and 2.[14] With a commercial antibody, HMCN1 was also reported to be present in the GBM of mice.[15] However, these antibodies did not show HMCN1 and 2 to be in a track pattern, nor were they authenticated by any further experiments, e.g., assayed in mice lacking HMCN1 or 2.

HMCN1 was identified as a normal matrix component in one proteomic analysis of human glomeruli, but not in a subsequent analysis.[16,17] Here we generated CRISPR/Cas9-mediated *Hmcn1* and *Hmcn2* knockout mice to test whether HMCNs function to join the two separate epithelial and endothelial BMs into the thick GBM during glomerulogenesis, and to confirm a previous report that the lack of HMCN1 causes preimplantation lethality,[18] a phenotype that has not been observed in other mammalian extracellular matrix gene mutants. In contrast to the reported lethality, we found *Hmcn1*$^{-/-}$ mice to be viable and fertile and to have no discernable defects. We also examined the normal localization of mouse HMCN1 with new antibodies using *Hmcn1* knockout mice as negative controls.

2 | RESULTS

2.1 | Production of HMCN1 antisera

To localize and investigate potential functions for HMCN1, we raised several different HMCN1 antisera in rabbits by immunizing with four recombinant partial human HMCN1 proteins: 1) the N-terminal VWA domain, 2) the thrombospondin type (TSP) 1 repeats, 3) the G2 nidogen domain, and 4) the C-terminal EGF and fibulin type modules.[4] Among these, antibodies to the VWA domain, to the TSP1 repeats, and to the C-terminus showed the same patterns of immunoreactivities to mouse tissues that were absent in *Hmcn1*$^{-/-}$ mice. Data shown in this report were obtained with the antiserum made to the C-terminus.

2.2 | Generation of *Hmcn1*$^{-/-}$ mice

To validate the antibodies, to investigate the function of HMCN1, and to confirm the previously reported preimplantation lethality,[18] we generated three different CRISPR/Cas9-mediated *Hmcn1* gene knockout alleles that carry frameshift mutations shortly after the translational start codon, leading to a DNA sequence encoding only 20-22 amino acids from the wild-type (WT) reading frame (Figure 1) plus an additional 5-26 amino acids from an incorrect reading frame, as compared to the complete >5,000 amino acids of HMCN1. If any downstream methionine codons would be used to begin translation, the resulting protein would lack a secretion signal peptide. Unlike the reported lethality, [18] our *Hmcn1*$^{-/-}$ mice were viable and fertile and did not show gross phenotypes.

2.3 | Deposition of HMCN1 in kidney

Our initial studies focused on the kidney glomerulus, because the mature glomerular basement membrane (GBM) of the kidney's filtration barrier results from fusion of two

separate BMs during glomerulogenesis[19,20] that could be mediated by a B-LINK-type complex containing HMCN1. Although deposition of HMCN1 in the GBM has been reported by others,[15] our immunostaining data showed deposition of HMCN1 in the mesangial matrix of glomeruli of aged mice but not in the GBM (Figure 2A). The signals were less intense in *Hmcn1*$^{+/-}$ kidney versus WT and undetectable in *Hmcn1*$^{-/-}$ kidney (Figure 2A), which demonstrates the specificity of the antiserum. The mesangial deposition of HMCN1 in younger adults varied (data not shown). In kidney of 2.5 day-old mice, HMCN1 was not detectable in developing glomeruli (data not shown), but it was present in the mesangial matrix of mature glomeruli (Figure 2B). Bright HMCN1signals were also detected in kidney arteries, veins, and smaller blood vessels (Figure 2B). Consistent with the lack of HMCN1 in the normal GBM, *Hmcn1*$^{-/-}$ mice through 10 months of age did not exhibit increased levels of protein in the urine, one expected consequence of a GBM defect (data not shown). Furthermore, HMCN1 deficiency in *Col4a5* null mice that model human Alport syndrome[21] did not aggravate the proteinuria or the GBM defects (data not shown). These data suggest that HMCN1 is not required for glomerular functions.

2.4 | HMCN1 tracks in whisker and hair follicles

HMCN1 was detected in several mouse tissues in distinct tracks, similar to the pattern observed in worms. In adult whisker follicles there are sinuses enveloped by a connective tissue sheath (Figure 3A, C). At the center of the follicle lies the whisker shaft, which is surrounded by the inner root sheath and the outer root sheath, the latter of which is abutted by a thick BM (Figure 3B). HMCN1 tracks were detected in the connective tissue sheath and along the BM of the outer root sheath (Figure 3A–H), with the tracks being most closely associated with the BM at the swelling of the root sheath below the ring sinus (Figure 3E). Whole-mount immunofluorescence of dissected whisker follicles displayed well organized HMCN1 tracks (Movie 1).

Similarly, HMCN1 tracks were associated with and formed into a woven network along the BM of hair follicles present on the whisker pad (Figure 3I, J) as well as those on the back and tail skin (data not shown). In contrast, HMCN1 was undetectable in *Hmcn1*$^{-/-}$ whisker or hair follicles (Figure 3K–M). Unlike in adult mice, in young pups HMCN1 also formed tracks in the dermis (Figure 3N), dermal papilla, and blood vessels (not shown) of both the skin and whisker pads. In a human skin biopsy, fine HMCN1 tracks were observed in hair follicles (Figure 3O, P) and in the dermis, which extended into the papillary regions (Figure 3Q). Although HMCN1 formed distinct structures in whisker and hair follicles, *Hmcn1*$^{-/-}$ mice did not exhibit defects in hair shaft adherence, as determined by a simple adhesive tape assay.[22] In addition, there were no overt defects in whisker length in *Hmcn1*$^{-/-}$ mice (data not shown).

2.5 | HMCN1 tracks in eyes

Human *HMCN1* has been implicated as associated with age related macular degeneration.[23,24] We therefore investigated the localization of HMCN1 in the mouse eye. Flat-mount immunofluorescence of dissected WT adult eye cups revealed distinct HMCN1 tracks in the scleral regions that border the cornea (Figure 4B–D; anterior cup) and surround the optic nerve head (Figure 4E–G; posterior cup). The HMCN1 tracks in the anterior part of the eye

were restricted to the inner scleral layers anterior to the retina, as revealed in sections, compared to the broad scleral and corneal domains of microfibril-associated glycoprotein 1 (MAGP1) (Figure 4H–M). Similarly, the HMCN1 tracks formed around the optic nerve head were also confined to the inner scleral layers abutting the choroid (Figure 4N–P). Weak HMCN1 signals were also detected in the corneal stroma (Figure 4I) and Bruch's membrane (data not shown). HMCN1 was undetectable in *Hmcn1*$^{-/-}$ eyes (Figure 4P). As in adult mice, HMCN1 tracks in the sclera of young pups were detected in regions bordering the cornea (Figure 4Q) and in those around the optic nerve head (data not shown). In young pups' eyes, HMCN1 tracks were also detected in the ciliary body (Figure 4Q), in the corneal stroma with stronger signals toward the corneal epithelium (Figure 4R), in the choroid, and in Bruch's membrane (Figure 4S). *Hmcn1*$^{-/-}$ mice did not show gross eye phenotypes. Physiological assays were not performed to investigate possible vision defects in *Hmcn1*$^{-/-}$ mice.

2.6 | HMCN1 tracks in the tongue

In WT adult tongue, HMCN1 tracks were detected along the BM of surface epithelial cells on both the dorsal (Figure 5A) and ventral (not shown) surfaces, and in the core of taste buds (Figure 5A). In WT pup tongue, HMCN1 tracks were abundant in the core of taste buds and were additionally detected in the connective tissue (Figure 5B) and in blood vessels (not shown). HMCN1 was undetectable in *Hmcn1*$^{-/-}$ tongue (Figure 5C). *Hmcn1*$^{-/-}$ mice did not show altered morphology of the tongue (Figure 5D–F). Assays were not performed to investigate possible functional defects in *Hmcn1*$^{-/-}$ tongue.

2.7 | HMCN1 tracks in the spleen and lymph nodes

HMCN1 formed discrete tracks in splenic and lymph node conduits, which form a network of small diameter tubes for transporting antigens and cytokines in secondary lymphoid organs. These conduits have a defined cell/extracellular matrix architecture consisting of stromal cells covering a BM that surrounds a layer of microfibrils enwrapping collagen fibers in the lumen of the conduit (Figure 5P).[25,26] In the spleens of WT and *Hmcn1*$^{+/-}$ mice, HMCN1 tracks were detected in conduits within the T-cell zone (Figure 6A) and in the capsule and trabeculae (Figure 6D). No such HMCN1 immunoreactivities were observed in *Hmcn1*$^{-/-}$ spleens (Figure 6E, H). HMCN1 tracks in T-cell zone conduits were enwrapped by the ER-TR7-positive microfibril layer (Figure 6C) and the collagen IV- and nidogen-positive BM (not shown), indicating localization of HMCN1 in the lumen of the conduit. Consistent with this, HMCN1 tracks were intertwined with or parallel to the collagen I bundles that filled the lumen of splenic conduits (Figure 6B, G).

In contrast to the T-cell zone of the spleen, HMCN1-positive conduits in lymph nodes were detected mainly in the B-cell follicles (Figure 6I). As in the spleen, HMCN1 tracks in lymph nodes were also associated with collagen I bundles in the lumen of conduits (Figure 6J, O). Airyscan Z-stack images of lymph nodes validated the localization of HMCN1 tracks in the lumen of conduits, as the tracks were enclosed by the ER-TR7-positive microfibril layer that was surrounded by the collagen IV-positive BM (Figure 6K, L).

One function of lymphoid conduits is to serve as a molecular sieve for small molecules to control their entry and flow through them.[26–28] To examine whether HMCN1 deficiency affected the accessibility of fluid and its contents to conduits, tracers of different sizes were injected into control and mutant mice and monitored for their passage in conduits of the draining lymph nodes and of the spleen.[27,28] Eight to 15 min after subcutaneous injection into footpads, control mice showed abundant distributions of injected 40- and 70-kD dextran molecules and bovine serum albumin (BSA, 68 kD) in conduits of the draining lymph nodes, in both the B-cell follicles and T-cell zones (B-cell follicles shown in Figure 7A–H). In contrast, the amount of injected immunoglobulin G (IgG, 150 kD) in lymph node conduits was low (Figure 7I, J), although injected IgG was detected in the cortical ridge, similar to the other three tracers examined (not shown). The distributions of all these tracers in *Hmcn1*$^{-/-}$ lymph nodes were similar to controls (Figure 7A–L). When the spleen was examined 10 min after retroorbital (intravenous) injection, both control and *Hmcn1*$^{-/-}$ mice displayed signals of 40- and 70-kD dextran molecules and BSA in splenic conduits, but IgG was undetectable (data not shown). Consistent with these data, HMCN1 deficiency did not affect the production of antibodies 1 or 2 weeks after immunization with either ovalbumin (48 kDa) or the much larger human laminin-511 trimer (~800 kDa) (Figure 7M).

2.8 | *Hmcn1* and *Hmcn2* double knock-out mice

To investigate the function of HMCN2 and whether HMCN2 might be compensating for the loss of HMCN1, we also generated three different CRISPR/Cas9-mediated *Hmcn2* knockout alleles with frameshift mutations downstream of the translational start codon, leading to a DNA sequence encoding only 42 or 43 amino acids (Figure 1) plus an additional 7-11 amino acids from an incorrect reading frame, as compared to the full-length HMCN2 of >5,000 amino acids. Like *Hmcn1*$^{-/-}$ mice, *Hmcn2*$^{-/-}$ mice were viable and fertile and did not show gross phenotypes. We do not have an antibody to HMCN2 to localize it in WT mice or to verify its absence in the mutant mice. When *Hmcn2*$^{-/-}$ mice were crossed to *Hmcn1*$^{-/-}$ mice to generate double knockouts, there were still no overt phenotypes, and the mice were viable and fertile.

3 | DISCUSSION

Using new antibodies raised against various modules of human HMCN1 that were authenticated with newly generated *Hmcn1* knockout mice, we have shown that HMCN1 localizes primarily in a track pattern in the extracellular matrix, similar to HMCN patterning in *C. elegans.*[2] HMCN1 assembled into fine tracks in adult mice, in some cases along a BM, in whisker follicles, hair follicles, the sclera of eyes, and within lymphoid conduits. HMCN1 tracks were more widespread in tissues of young versus adult mice. For example, the HMCN1 tracks in the dermis, in the corneal stroma, and in the core of taste buds in young pups became undetectable or less distinct in adult mice. In addition, HMCN1 was found in the glomerular mesangial matrix in kidneys of aged mice and young pups. This is in contrast to the reported presence of HMCN1 in the kidney GBM as shown using a commercial HMCN1 antibody[15] that is no longer available. Deposition of HMCN proteins was also reported in the pericellular matrix of epithelial cells in mouse skin and tongue using an antibody that was raised against *C. elegans* HMCN.[29] In contrast, our data were obtained

with antibodies raised against various domains of recombinant human HMCN1: the VWA domain, the TSP1 repeats, and the C-terminus. That all three of these antibodies detected the same track pattern of immunostaining on mouse tissues and were validated by the lack of reactivity in *Hmcn1* knockout mouse tissues is strong evidence for their specificity.

Studies in *C. elegans* show that HMCN has pleiotropic functions including regulating the attachment of specific mechanosensory neurons to the epidermis and the attachment and movement of intestine and uterus.[2,3] These forms of attachment by HMCN tracks occur between two specific BMs or are mediated by hemidesmosomes. However, the sites of HMCN1 deposition in mouse and human in our report were not between two BMs, but rather within or along the BM, as observed in whisker and hair follicles. In contrast to the adult mouse skin, the young pup and human skin showed additional HMCN1 tracks in the dermis, with some tracks extending into the epidermal BM where they might be in contact with hemidesmosomes, as observed in *C. elegans*. The other locations of HMCN1 tracks identified in adult mice in our report include the connective tissue sheath of whisker follicles, the sclera of eyes, the lumen of some conduits in the spleen and lymph nodes, and the capsule and trabeculae of the spleen, all of which are enriched in collagen fibers. In young pups, HMCN1 tracks were also identified in several other collagen-rich tissues such as the corneal stroma, the choroid, and Bruch's membrane of the eyes; the connective tissues of the tongue; and blood vessels of the kidney. It remains to be determined how HMCN1 is assembled into tracks and how these tracks interact with sheet-forming collagens in the BM, fibrillar collagens in connective tissues, and other extracellular matrix components. In contrast, HMCN1 deposition in the mesangial matrix of the kidney was not organized into a track pattern. This can be attributed to the amorphous nature of the mesangial matrix versus the more structured matrices in the BM and connective tissues.

That HMCN1 proteins assemble into tracks suggests a role for HMCN1 in structural support. Data from a mouse model of myocardial infarction and from cultured cardiac fibroblasts suggest that HMCN1 functions in myocardial remodeling by regulating pro-fibrotic TGB-β responses [30,31]. It is possible that HMCN1 also plays important roles in remodeling of the tissues examined in our study during development and in response to injury.

In contrast to the early embryonic lethality of *Hmcn1*$^{-/-}$ mice reported by others,[18] our CRISPR/Cas9-mediated *Hmcn1* knockout mice were viable and fertile. These mice did not show abnormalities in the several organs where HMCN1 was deposited. For example, HMCN1 deficiency did not affect the adherence or growth of coat hairs and whiskers, the sieving function of conduits in the spleen and lymph nodes, or the immune response to injected antigens. However, assays were not performed to investigate possible functional defects in eye and tongue. The lack of distinct phenotypes in *Hmcn1*$^{-/-}$ mice is unlikely due to expression of a truncated protein, as the antibodies against the N-terminal VWA domain and the TSP1 repeats were not immunoreactive with *Hmcn1*$^{-/-}$ tissues (data not shown), as shown for the antibody against the C-terminus (Figures 2–6). Similarly, *Hmcn2*$^{-/-}$ mice were also viable and fertile and did not show overt phenotypes. Furthermore, HMCN2 deficiency did not lead to any discernible phenotypes in *Hmcn1*$^{-/-}$ mice. It is possible that HMCN2 is normally deposited at different locations than HMCN1, which will remain

unknown until a HMCN2-specific antibody becomes available. In zebrafish, *Hmcn1* and *Hmcn2* genes are expressed in distinct tissue domains. *Hmcn1* knockout fish manifest massive fin blistering,[11] whereas *Hmcn2* knockdown neither leads to discernible phenotypes nor aggravates fin blistering in *Hmcn1* mutants.[12] However, double knockdown of *Hmcn2* and *fibulin-1*, both of which are expressed in the same tissue domains, leads to blistering defects.[12] It remains to be investigated whether the lack of mouse HMCN1 is compensated for by one of the six other members of the fibulin family [32].

Our results differ significantly from the previous report of early preimplantation lethality in *Hmcn1* mutant mice.[18] In that report, *Hmcn1* expression was inhibited in three different ways: gene knockout via homologous recombination in embryonic stem cells to generate homozygous mutants; production of haploid *Hmcn1*-null parthenogenotes; and gene knockdown using siRNA. It is possible that the discrepancies between our and their data result from knocking out different isoforms of HMCN1, though there is no clear evidence to support this. Identification of a complete set of HMCN1 isoforms may provide insights into the discrepancies.

4 | EXPERIMENTAL PROCEDURES

4.1 | Production of HMCN1 antibodies

The VWA domain, TSP1 repeats (position 4526-4869), and EGF1-8 and fibulin domains of human HMCN1 (accession: NP_114141) were recombinantly expressed in HEK 293 cells using the pCEP-Pu vector containing BM-40 signal peptide[33]. Purified proteins were used to immunize rabbits. Antibodies raised against the VWA domain were affinity-purified using proteins containing the VWA domain[34]. Antibodies raised against the EGF1-8 and fibulin domains were affinity-purified using the EGF1-6 fragment (position 5107-5413) of furin-cleaved EGF1-8 and fibulin domains.

4.2 | Generation of *Hmcn1* knockout mice

The *Hmcn1* and *Hmcn2* knockout alleles were generated by CRISPR/Cas9-initiated non-homologous end-joining. The guide RNAs used for *Hmcn1* (5'-CGTTCTTCCCTAGCTGGAGA-3') and *Hmcn2* (5'-GCCGGTGACATCGAAGACGA-3') were designed by the Washington University Transgenic Vectors Core and microinjected into B6CBAF2/J pronuclei along with Cas9 mRNA by the Washington University Mouse Genetics Core. Founders carrying frame shift mutations were identified by next generation sequencing of PCR products derived from genomic DNA extracted from toe biopsies. Mutant founders were mated with B6CBAF1/J mice to produce three independent *Hmcn1+/−* and three independent *Hmcn2+/−* heterozygotes. Homozygous and compound heterozygous *Hmcn1* and *Hmcn2* knockout mice were generated by crossing heterozygotes. Double knockout *Hmcn1*; *Hmcn2* mice were generated by standard breeding. All animal procedures were approved by the Washington University Animal Studies Committee.

4.3 | Immunofluorescence on tissue sections

Frozen sections were prepared by embedding tissues in OCT compound (Sakura Finetek, Torrance, CA), sectioning at 7 μm in a cryostat, and air-drying. After fixation in cold acetone

at −20C for 10 min followed by rehydration in PBS and blocking in 1% BSA in PBS, sections were incubated in primary antibodies for 1 h, in fluorochrome-conjugated secondary antibodies (Invitrogen in Thermo Fisher Scientific, Rockford, IL) with Hoechst 33258 as a nuclear counterstain for 30 min, and then mounted in 90% glycerol in 0.1X PBS and 1 mg/ml para-phenylenediamine. Dilutions of primary antibodies used were as follows: 1:600 for HMCN1; 1:1,000 for nidogen clone ELM1, 1:500 for LAMA5 clone 4C7 (both from MilliporeSigma, Burlington, MA); 1:200 for MAGP1 (a gift from Robert Mecham); 1:400 for CD3e (BioLegend, San Diego, CA); 1:400 for B220 (eBioscience in Thermo Fisher Scientific); 1:100 for both collagen I & IV (SouthernBiotech, Birmingham, AL); and 1:500 for ER-TR7 (abcam, Cambridge, MA). Stained sections were viewed under a Nikon Eclipse E800 microscope, a Nikon C1 confocal system (Nikon Instruments, Melville, NY), or a Zeiss LSM 880 Airyscan confocal microscope (Carl Zeiss Microscopy, Thornwood, NY). Confocal images were analyzed and 3D-reconstructed in Nikon Elements software. Airyscan confocal images were analyzed by Zeiss Zen Black software. Experiments using the human skin biopsy sample were approved by the Washington University in St. Louis Institutional Review Board (protocol numbers 201507042 and 201412117).

4.4 | Whole-mount immunofluorescence

Whisker follicles were resected from the whisker pad of adult mice and cut open by removing the connective tissue sheath from one side. The scleral flat mounts from adult mice were prepared as previously described.[35] Briefly, mouse eyes were resected with the external tissue and optic nerve removed, excised into anterior and posterior cups, and flattened by making 4 to 5 incisions along the longitudinal circle with the lens, retina, and choroid removed. The prepared samples were permeabilized for 3 h in blocking buffer (1% BSA, 0.2% skim milk, and 0.3% Triton X-100 in PBS), incubated at 4C overnight in primary antibodies, incubated for 2 h in fluorochrome-conjugated secondary antibodies, post-fixed for 30 min in 4% paraformaldehyde in PBS, and then mounted in glycerol as above. The primary antibodies used were twice as concentrated as those for immunofluorescence on tissue sections. Z-stack images were acquired with a Nikon C1 confocal system. The analysis and 3D reconstruction were performed by Nikon Elements software.

4.5 | Analysis of tracer distribution

To examine tracer distribution in draining lymph nodes, mice at 7 to 9 months of age (~35 g) were injected into footpads subcutaneously with 20 μl of a mixture of lysine-fixable, 40 kDa dextran-fluorescein and 70 kDa dextran-TMR (5 mg/ml each; Invitrogen) or of a mixture of BSA-FITC (68 kDa, 2.5 mg/ml; MilliporeSigma) and goat anti-rabbit IgG (150 kDa, 1 mg/ml; Invitrogen). At 8-15 min after injection, axillary and brachial lymph nodes and popliteal lymph nodes were collected from forelimb and hindlimb injections, respectively, with inguinal lymph nodes collected as negative controls. Lymph nodes were fixed in 4% paraformaldehyde in PBS, equilibrated in 10% and then in 30% sucrose in PBS at 4°C for 1 h and overnight, respectively, and embedded and sectioned as above. Sections were then fixed in 4% paraformaldehyde in PBS, and counterstained and mounted as above. To examine tracer distribution in the spleen, mice were intravenously injected retroorbitally

with 150 μl of tracer mixtures as above. At 10-15 min after injection, the spleen was collected and processed as was performed with lymph nodes.

4.6 | Analysis of induction of immune response

Mice at 9 to 10 months of age were injected intraperitoneally with ovalbumin (MilliporeSigma) or human laminin-511 (BioLamina, Sundbyberg, Sweden) daily at 5 mg/kg and 0.15 mg/kg, respectively, for 3 days. Blood samples were collected prior to immunization and at 1 and 2 weeks after immunization. Plasma was then collected, diluted at 50 and 1,000 fold for ovalbumin and human laminin-511 immunization, respectively, and assayed for antibody titers by ELISA.

4.7 | Statistical analysis

Two-tailed, unpaired Student's *t*-tests were used to determine statistical significance in the quantification assays. Differences were considered significant with $P<0.05$.

Supplementary Material

Refer to Web version on PubMed Central for supplementary material.

ACKNOWLEDGMENTS

We thank Renate Lewis of the Transgenic Vectors Core for design and validation of the guide RNAs, the Mouse Genetics Core for generating the knockout mice and for mouse husbandry and urine collections, and Jennifer Richardson for genotyping the mice. We also thank Brian Kim for providing the human skin biopsy sample, Yoav Segal for providing *Col4a5* mutant mice, and Alexander Nystrom, Gwendalyn Randolph, Rafa Sanguinetti Czepielewski, and Emma Erlich for helpful discussions. This work was funded by NIH grants R01DK078314 to JHM and R35GM118049 to DRS.

Grant support: NIH: R01DK078314 and R35GM118049

REFERENCES

1. Argraves WS, Greene LM, Cooley MA, Gallagher WM. Fibulins: physiological and disease perspectives. Embo Reports. 2003;4:1127–1131. [PubMed: 14647206]
2. Vogel BE, Hedgecock EM. Hemicentin, a conserved extracellular member of the immunoglobulin superfamily, organizes epithelial and other cell attachments into oriented line-shaped junctions. Development. 2001;128:883–894. [PubMed: 11222143]
3. Vogel BE, Muriel JM, Dong C, Xu X. Hemicentins: what have we learned from worms? Cell Res. 2006;16:872–878. [PubMed: 17031392]
4. Xu X, Xu M, Zhou X et al. Specific structure and unique function define the hemicentin. Cell Biosci. 2013;3:27. [PubMed: 23803222]
5. Muriel JM, Dong C, Hutter H, Vogel BE. Fibulin-1C and Fibulin-1D splice variants have distinct functions and assemble in a hemicentin-dependent manner. Development. 2005;132:4223–4234. [PubMed: 16120639]
6. Sherwood DR, Plastino J. Invading, Leading and Navigating Cells in Caenorhabditis elegans: Insights into Cell Movement in Vivo. Genetics. 2018;208:53–78. [PubMed: 29301948]
7. Morrissey MA, Keeley DP, Hagedorn EJ et al. B-LINK: a hemicentin, plakin, and integrin-dependent adhesion system that links tissues by connecting adjacent basement membranes. Dev Cell. 2014;31:319–331. [PubMed: 25443298]
8. Dong C, Muriel JM, Ramirez S et al. Hemicentin assembly in the extracellular matrix is mediated by distinct structural modules. J Biol Chem. 2006;281:23606–23610. [PubMed: 16798744]

9. Whittaker CA, Hynes RO. Distribution and evolution of von Willebrand/integrin A domains: widely dispersed domains with roles in cell adhesion and elsewhere. Mol Biol Cell. 2002;13:3369–3387. [PubMed: 12388743]
10. Keeley DP, Sherwood DR. Tissue linkage through adjoining basement membranes: The long and the short term of it. Matrix Biol. 2019;75-76:58–71. [PubMed: 29803937]
11. Carney TJ, Feitosa NM, Sonntag C et al. Genetic analysis of fin development in zebrafish identifies furin and hemicentin1 as potential novel fraser syndrome disease genes. PLoS Genet. 2010;6:e1000907. [PubMed: 20419147]
12. Feitosa NM, Zhang J, Carney TJ et al. Hemicentin 2 and Fibulin 1 are required for epidermal-dermal junction formation and fin mesenchymal cell migration during zebrafish development. Dev Biol. 2012;369:235–248. [PubMed: 22771579]
13. Abrahamson DR. Origin of the glomerular basement membrane visualized after in vivo labeling of laminin in newborn rat kidneys. J Cell Biol. 1985;100:1988–2000. [PubMed: 3889015]
14. Xu X, Dong C, Vogel BE. Hemicentins assemble on diverse epithelia in the mouse. J Histochem Cytochem. 2007;55:119–126. [PubMed: 17015624]
15. Toffoli B, Zennaro C, Winkler C et al. Hemicentin 1 influences podocyte dynamic changes in glomerular diseases. Am J Physiol Renal Physiol. 2018;314:F1154–F1165. [PubMed: 29488390]
16. Hobeika L, Barati MT, Caster DJ, McLeish KR, Merchant ML. Characterization of glomerular extracellular matrix by proteomic analysis of laser-captured microdissected glomeruli. Kidney Int. 2017;91:501–511. [PubMed: 27988214]
17. Lennon R, Byron A, Humphries JD et al. Global analysis reveals the complexity of the human glomerular extracellular matrix. J Am Soc Nephrol. 2014;25:939–951. [PubMed: 24436468]
18. Xu X, Vogel BE. A secreted protein promotes cleavage furrow maturation during cytokinesis. Curr Biol. 2011;21:114–119. [PubMed: 21215633]
19. Miner JH. Organogenesis of the kidney glomerulus: Focus on the glomerular basement membrane. Organogenesis. 2011;7.
20. Abrahamson DR. Structure and development of the glomerular capillary wall and basement membrane. Am J Physiol. 1987;253:F783–794. [PubMed: 3318497]
21. Rheault MN, Kren SM, Thielen BK et al. Mouse model of X-linked Alport syndrome. J Am Soc Nephrol. 2004;15:1466–1474. [PubMed: 15153557]
22. Lin MH, Leimeister C, Gessler M, Kopan R. Activation of the Notch pathway in the hair cortex leads to aberrant differentiation of the adjacent hair-shaft layers. Development. 2000;127:2421–2432. [PubMed: 10804183]
23. McKay GJ, Clarke S, Hughes A et al. A novel diagnostic test detects a low frequency of the hemicentin Gln5345Arg variant among Northern Irish age related macular degeneration patients. Mol Vis. 2004;10:682–687. [PubMed: 15467524]
24. Schultz DW, Klein ML, Humpert AJ et al. Analysis of the ARMD1 locus: evidence that a mutation in HEMICENTIN-1 is associated with age-related macular degeneration in a large family. Hum Mol Genet. 2003;12:3315–3323. [PubMed: 14570714]
25. Lokmic Z, Lammermann T, Sixt M, Cardell S, Hallmann R, Sorokin L. The extracellular matrix of the spleen as a potential organizer of immune cell compartments. Semin Immunol. 2008;20:4–13. [PubMed: 18243017]
26. Sixt M, Kanazawa N, Selg M et al. The conduit system transports soluble antigens from the afferent lymph to resident dendritic cells in the T cell area of the lymph node. Immunity. 2005;22:19–29. [PubMed: 15664156]
27. Gretz JE, Norbury CC, Anderson AO, Proudfoot AE, Shaw S. Lymph-borne chemokines and other low molecular weight molecules reach high endothelial venules via specialized conduits while a functional barrier limits access to the lymphocyte microenvironments in lymph node cortex. J Exp Med. 2000;192:1425–1440. [PubMed: 11085745]
28. Nolte MA, Belien JA, Schadee-Eestermans I et al. A conduit system distributes chemokines and small blood-borne molecules through the splenic white pulp. J Exp Med. 2003;198:505–512. [PubMed: 12900524]

29. Thompson CL, Klein BE, Klein R et al. Complement factor H and hemicentin-1 in age-related macular degeneration and renal phenotypes. Hum Mol Genet. 2007;16:2135–2148. [PubMed: 17591627]

30. Chowdhury A, Hasselbach L, Echtermeyer F, Jyotsana N, Theilmeier G, Herzog C. Fibulin-6 regulates pro-fibrotic TGF-beta responses in neonatal mouse ventricular cardiac fibroblasts. Sci Rep. 2017;7:42725. [PubMed: 28209981]

31. Chowdhury A, Herzog C, Hasselbach L et al. Expression of fibulin-6 in failing hearts and its role for cardiac fibroblast migration. Cardiovasc Res. 2014;103:509–520. [PubMed: 24951538]

32. de Vega S, Iwamoto T, Yamada Y. Fibulins: multiple roles in matrix structures and tissue functions. Cell Mol Life Sci. 2009;66:1890–1902. [PubMed: 19189051]

33. Kohfeldt E, Maurer P, Vannahme C, Timpl R. Properties of the extracellular calcium binding module of the proteoglycan testican. FEBS Lett. 1997;414:557–561. [PubMed: 9323035]

34. Timpl R Antibodies to Collagens and Procollagens. Methods in Enzymology. 1982;82:472–498. [PubMed: 6176835]

35. Pijanka JK, Kimball EC, Pease ME et al. Changes in scleral collagen organization in murine chronic experimental glaucoma. Invest Ophthalmol Vis Sci. 2014;55:6554–6564. [PubMed: 25228540]

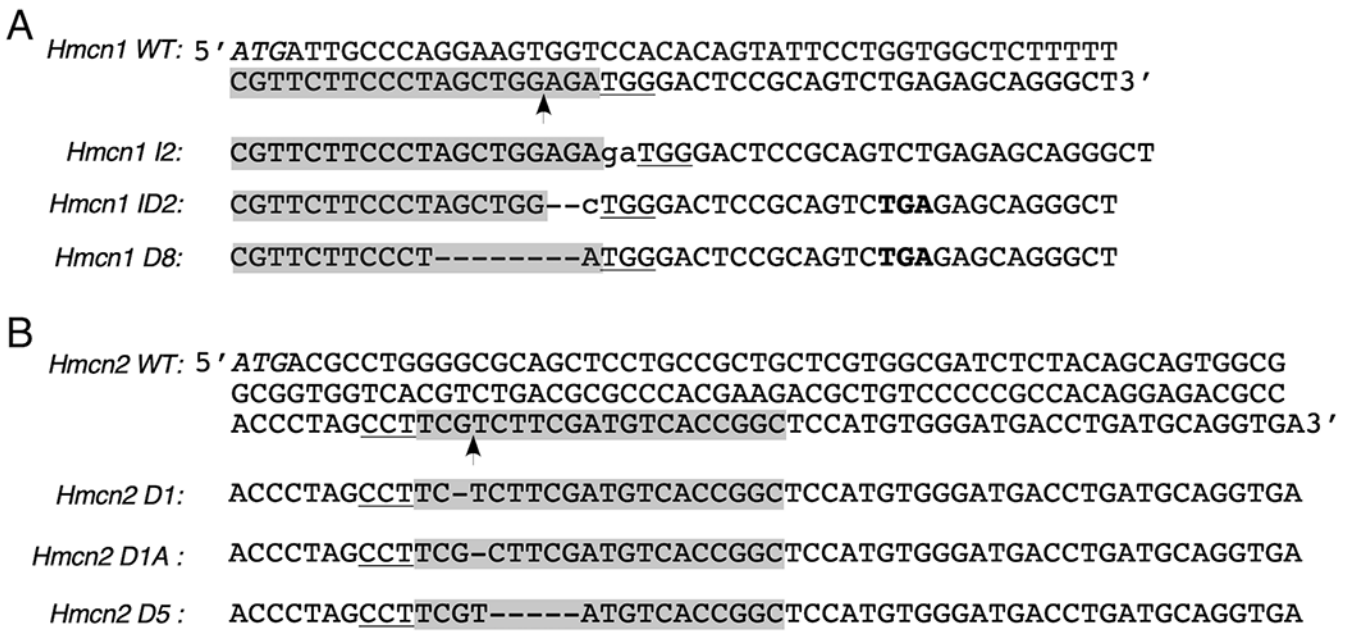

Figure 1. DNA sequences of *Hmcn*1 and *Hmcn2* mutations generated by CRISPR/Cas9.

The *Hmcn1* and *Hmcn2* knockout alleles were generated by CRISPR/Cas9-mediated non-homologous end-joining. Partial exon 1 sequences of WT *Hmcn1* (A) and *Hmcn2* (B) genes are shown at the top, and the knockout alleles are shown at the bottom. Guide RNA sequences are shadowed with the Cas9-cut site marked with an arrow. The protospacer adjacent motif NGG is underlined, and the protein translation initiation codon ATG is italicized. The guide RNA for *Hmcn2* is shown as an antisense sequence here. The insertions (lower case) and deletions (dash) in all mutant alleles and the premature stop codon TGA (bold) in *Hmcn1 ID2* and *D8* alleles are also marked.

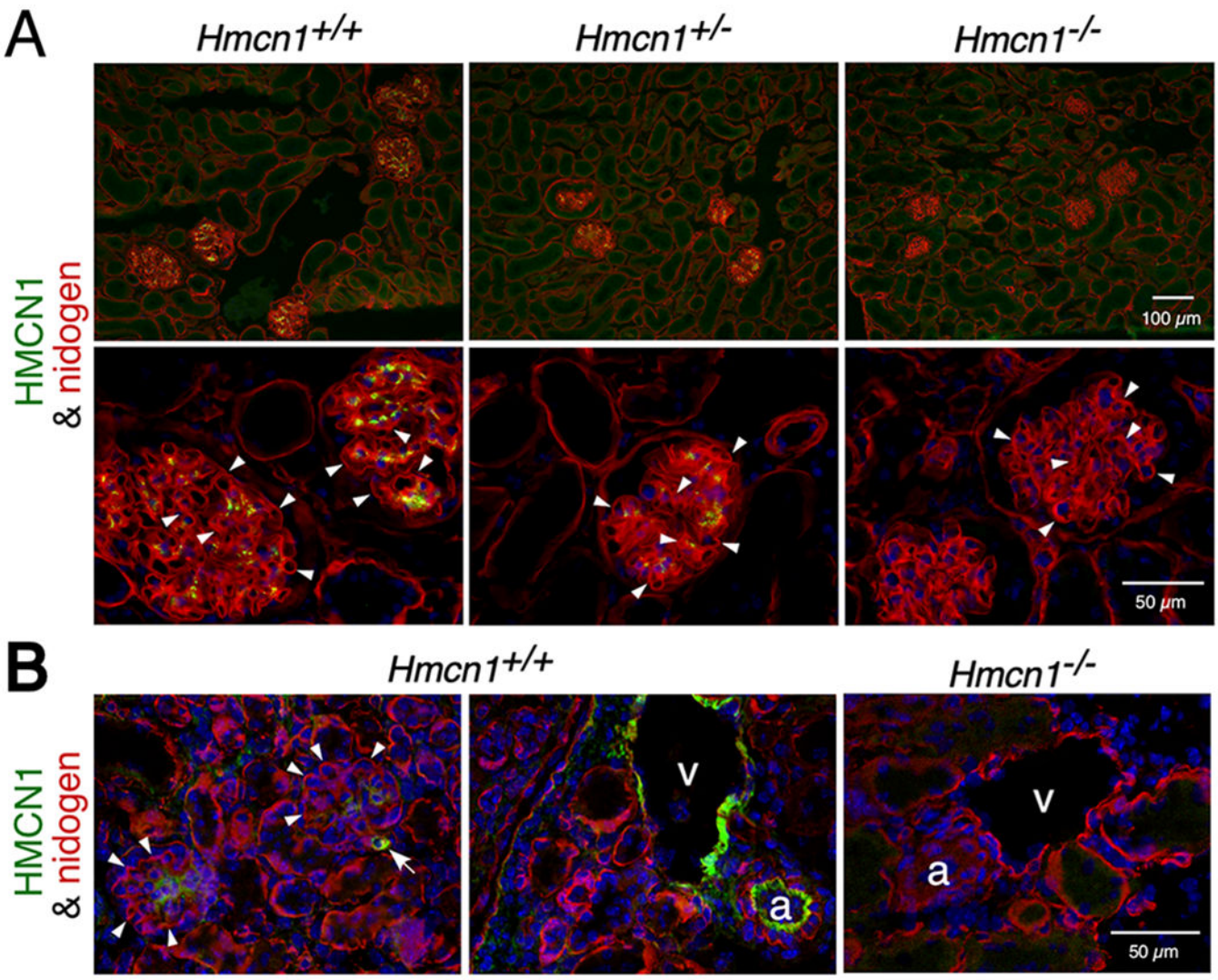

Figure 2. HMCN1 deposition in the kidney.

Kidney sections from mice at 10 months (A) and 2.5 days (B) of age with the genotypes indicated were subjected to immunofluorescence assays. (A) High magnification images are shown in the lower panels. WT and *Hmcn1*$^{+/-}$ adult kidneys showed deposition of HMCN1 (green) in the mesangial matrix of glomeruli. There was no HMCN1 detected in the nidogen-positive (red) GBM (arrowheads). There were no HMCN1 signals in *Hmcn1*$^{-/-}$ kidneys, demonstrating the specificity of the antibody. (B) Deposition of HMCN1 was detected in WT pups in the mesangial matrix, small blood vessels (arrow), artery (a), and vein (v) but undetectable in the GBM (arrowheads). *Hmcn1*$^{-/-}$ kidneys did not show signals.

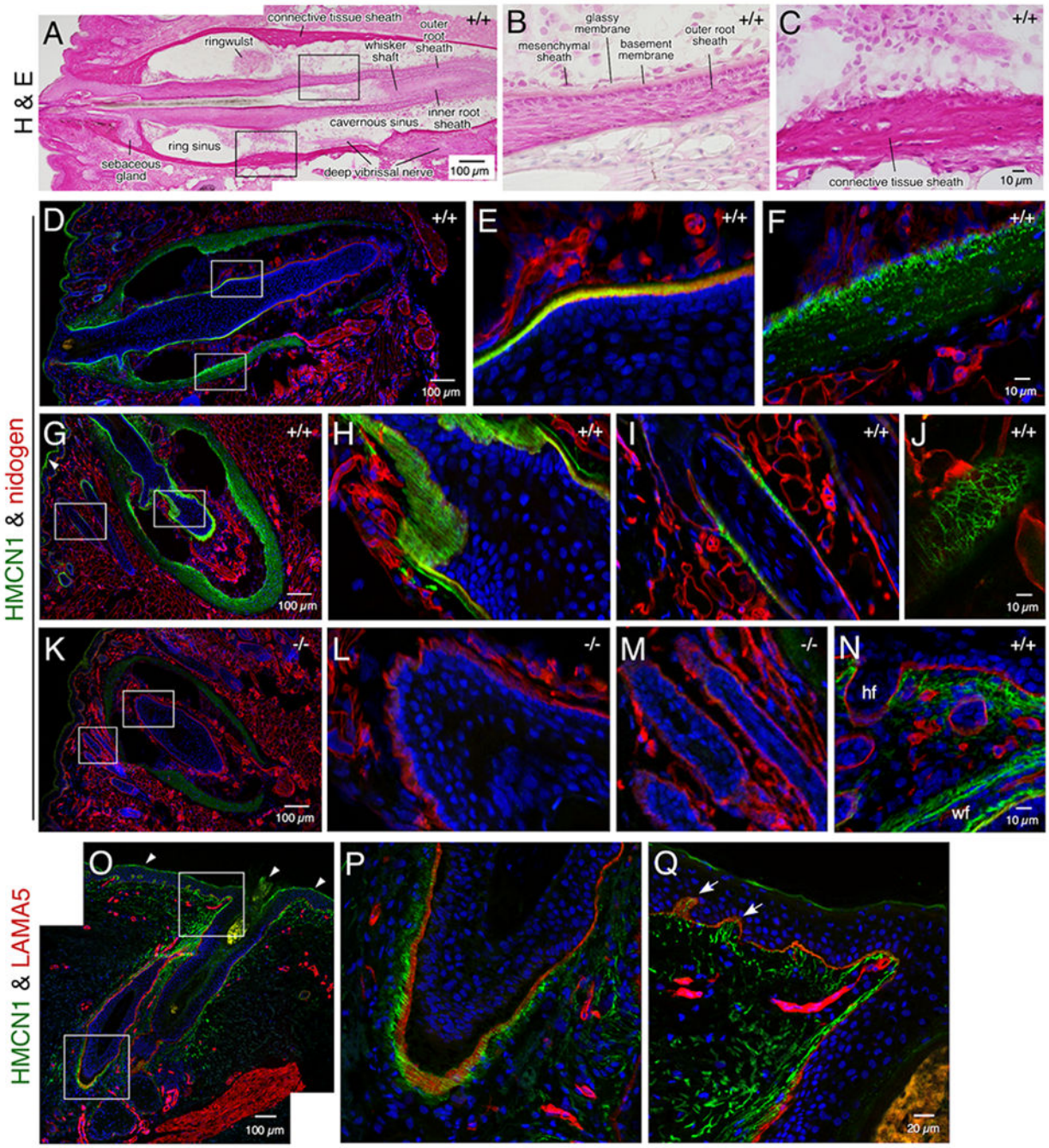

Figure 3. HMCN1 tracks in whisker and hair follicles.

Sections of mouse whisker pads at 8 months (A-M) and 2.5 days (N) of age (*Hmcn1* genotypes indicated) and a human skin biopsy (O-P) were subjected to hematoxylin & eosin staining or confocal immunofluorescence assays. The boxed regions in A, D, G, K, O are magnified in the two panels following each of them. HMCN1 was detected in WT adult mice in the BM of the outer root sheath (D, E) and in the connective tissue sheath (F) of whisker follicles, with distinct tracks observed along the BM in sections cut obliquely (G, H). HMCN1 tracks were also detected in hair follicles, along the BM (I) or in a reticular

pattern when viewed on the surface of hair follicles (J). There were no specific signals in *Hmcn1*$^{-/-}$ mice (K, L, M). In addition to hair follicles (hf) and whisker follicles (wf), HMCN1 signals were detected in the dermis of WT whisker pads of pups (N). (O-Q) HMCN1 tracks were found along the BM of human hair follicles (P) and in the dermis and its papillary structures (arrows in Q). Non-specific signals in G and O are marked (arrowheads).

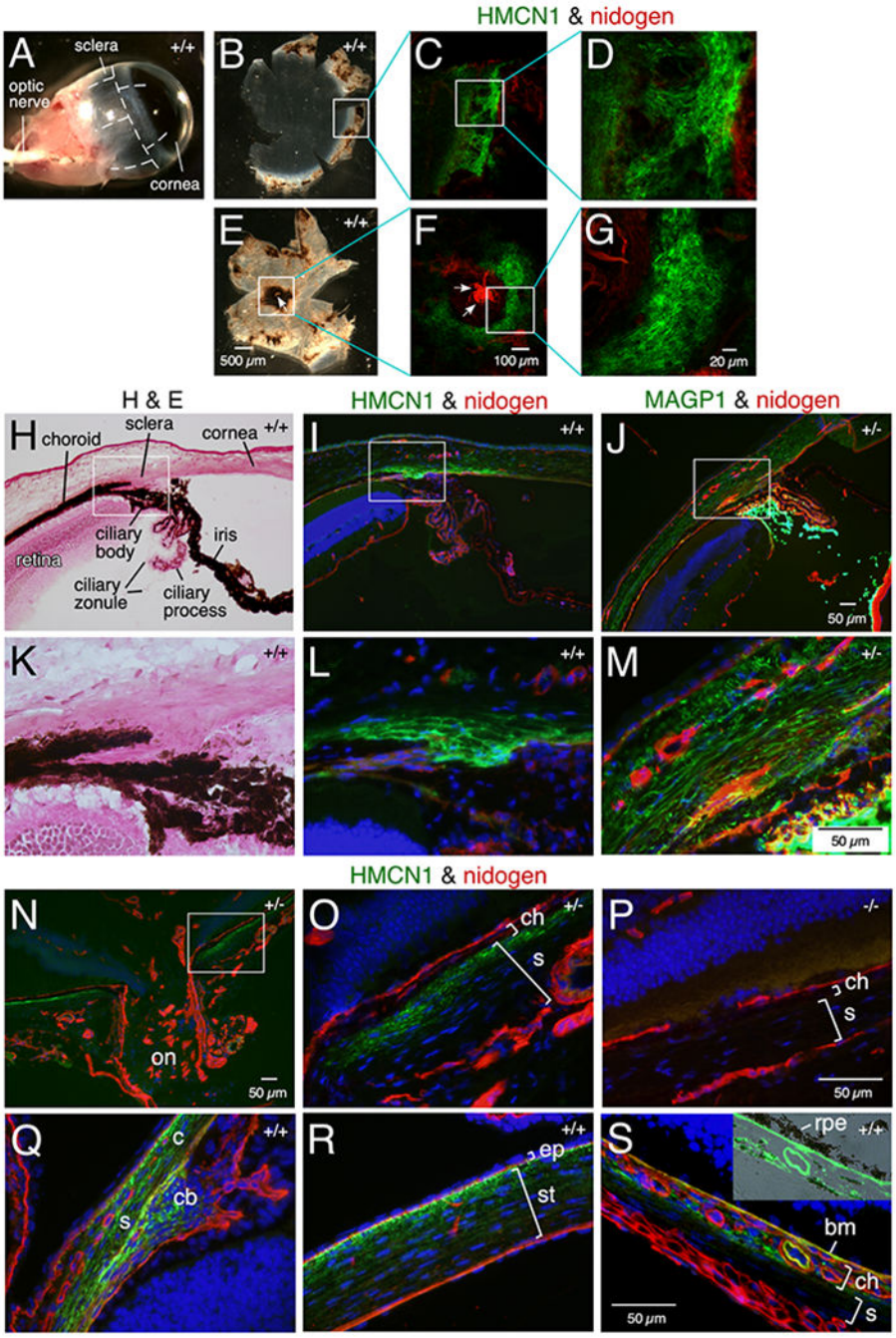

Figure 4. HMCN1 tracks in mouse eyes.

(A-G) WT eyes (11 months) were dissected along the dashed lines (A) to release anterior (B) and posterior (E) eye cups and subjected to immunofluorescence. HMCN1 tracks were detected in scleral regions bordering the cornea (C, D) and surrounding the optic nerve head (ONH) (F, G; arrows point to the ONH). (H-S) Sagittal sections of eyes at age 4 months (H-P) and 2.5 days (Q-S) with *Hmcn1* genotypes indicated were subjected to H&E staining or immunofluorescence. The boxed regions in H-J and N are magnified in K-M and O, respectively. Bright HMCN1 tracks were detected in inner scleral layers anterior to the retina

(I, L) with weaker signals in the cornea (I), compared to the broader expression domain of microfibril-associated glycoprotein 1 (MAGP1) in sclera and cornea (J, M). Bright MAGP1 staining marks ciliary zonules. The HMCN1 tracks detected around the ONH (on in N) were confined to the inner scleral layer (s) abutting the choroid (ch in O). There were no HMCN1 signals in *Hmcn1*$^{-/-}$ mice (P). In WT pup eyes, HMCN1 tracks were detected in scleral regions (s) bordering the cornea (c), in the ciliary body (cb in Q), in corneal stroma (st) with stronger signals toward the corneal epithelium (ep in R), in the choroid (ch), and in Bruch's membrane (bm), but tracks were undetectable in remaining scleral regions (s in S). Inset in S is an overlay of HMCN1 signals with the bright-field image, showing the HMCN1-stained Bruch's membrane abutting the retinal pigment epithelium (rpe).

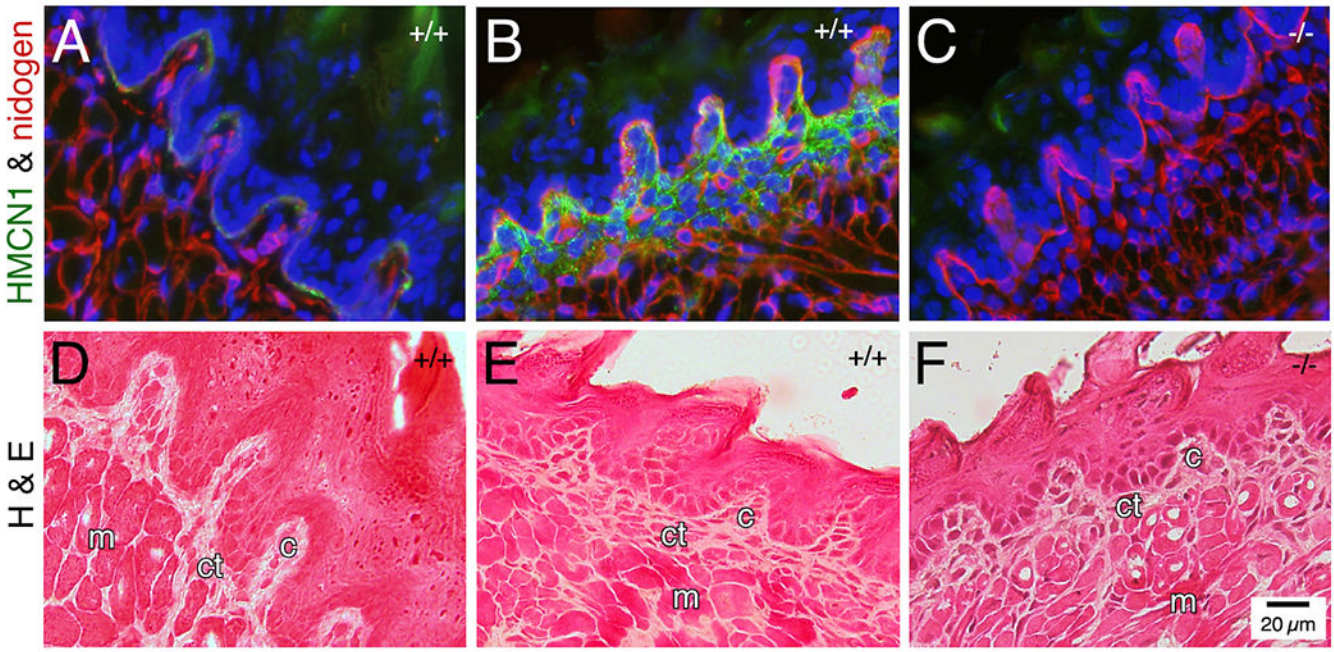

Figure 5. HMCN1 tracks in the tongue.

Tongue sections from mice at 3 months (A, D) and 2.5 days (B, C, E, F) of age were subjected to immunofluorescence assays (A-C) or hematoxylin & eosin staining (D-F). In WT adult tongue, HMCN1 was detected weakly along the epithelial BM and in the core of taste buds (A, D). In WT pup tongue, HMCN1 tracks were abundant in the core of taste buds and were additionally detected in the connective tissue (B, E). No HMCN1 was detected in *Hmcn1*$^{-/-}$ pups (C, F). c, core; ct, connective tissue; m, muscle. *Hmcn1* genotypes are designated in the upper right corner of each panel.

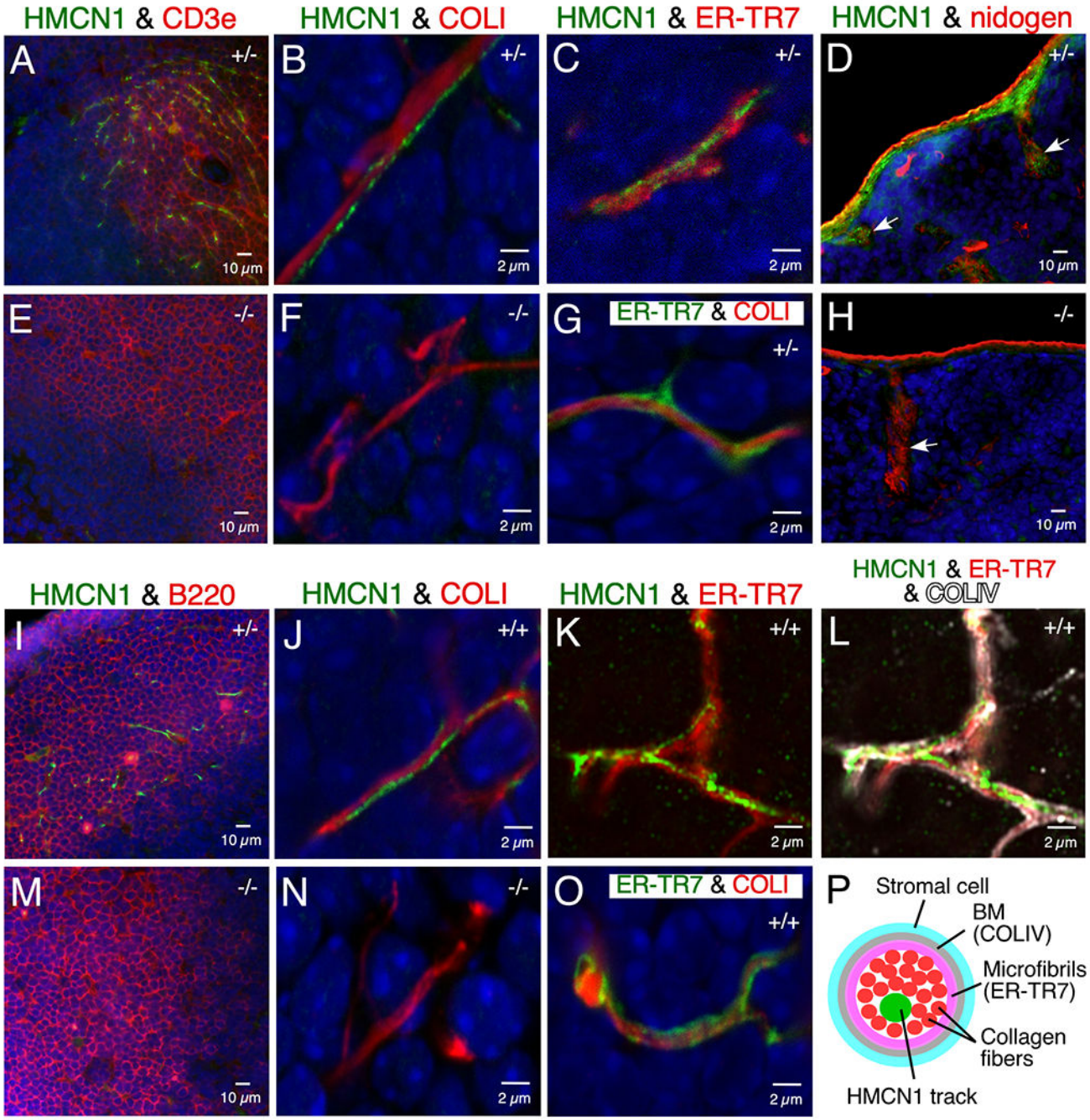

Figure 6. HMCN1 tracks in the spleen and lymph nodes.

Sections of mouse spleen (A-H) and lymph nodes (I-O) at 4 to 9 months of age were subjected to immunofluorescence. In spleen, HMCN1 (green) was detected in conduits of the T-cell zone marked by CD3e (A), enclosed by the ER-TR7-positive microfibril layer (C), and intertwined with or parallel to collagen I fibers in the lumen (B, G). HMCN1 also formed tracks in the capsule and trabeculae of the spleen (arrow in D). There was no HMCN1 signal in *Hmcn1*$^{-/-}$ mice (E, F, H). In inguinal (I) or popliteal (J-L, O) lymph nodes, HMCN1 (green) was detected in conduits of the B-cell follicles marked by B220 (I),

enclosed by the ER-TR7-positive microfibril layer (K) that was surrounded by the collagen IV-positive basement membrane (L), and associated with the collagen I fibers in the lumen (J, O), compared to no signals in *Hmcn1*$^{-/-}$ mice (M, N). Panels with a scale bar of 2 μm are all confocal images. K and L are Airyscan images of the same Z plane. *Hmcn1* genotypes are designated in the upper right corner of the panels. Panel P illustrates components of a lymphoid conduit in cross section.

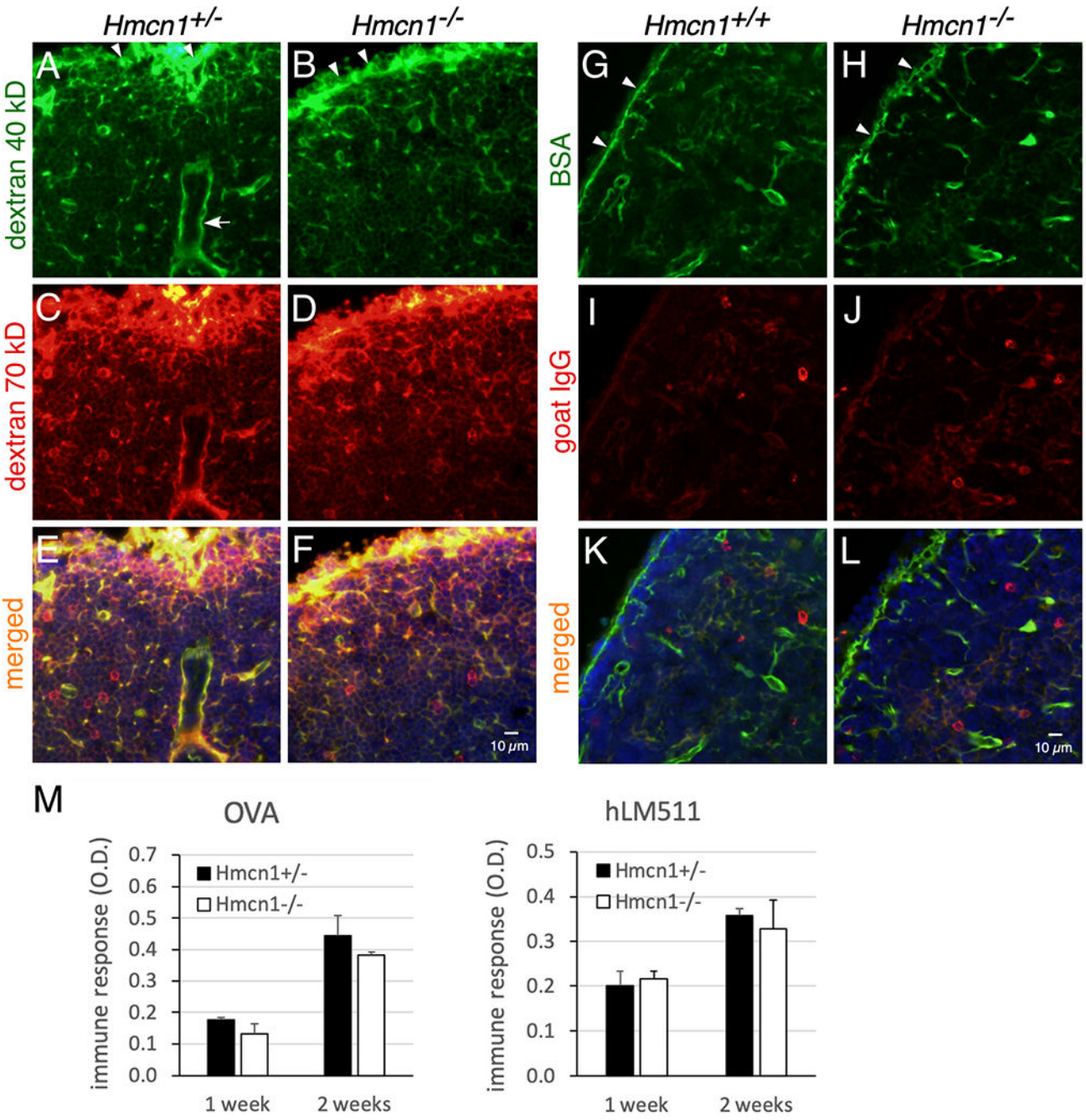

Figure 7. Analyses of effects of HMCN1 deficiency by tracer distribution and immune responses.

(A-L) Mice of the indicated genotypes at 7 to 9 months of age were injected subcutaneously into footpads with a mixture of 40-kD dextran-fluorescein and 70-kD dextran-TMR (A-F) or a mixture of BSA-FITC (68 kDa) and goat anti-rabbit-IgG-Cy3 (150 kDa) (G-L). Popliteal (A-F) and brachial (G-L) lymph nodes were collected at 15 and 9 min after injection, respectively, fixed, and then sectioned. (A-F) Injected 40- and 70-kDa dextrans were distributed in the subcapsular sinuses (arrowheads) and in conduits of B-cell follicles in both control and mutant mice. (G-L) Injected BSA was also distributed to subcapsular sinuses

and to conduits of B-cell follicles. In contrast, the distribution of goat IgG in the same lymph node was weak (I-L). Similar results were obtained for control and mutant mice. Arrow in A, high endothelial venule. (M) Mice at 9 to 10 months of age were immunized by intraperitoneal injections with ovalbumin (OVA) or human laminin-511 (hLM511) daily for 3 days. By ELISA control and *Hmcn1*$^{-/-}$ mice showed similar induction of antibodies to OVA or hLM511 at 1 and 2 weeks of immunization.